Title
Manipulating the Transition Dipole Moment of CsPbBr3 Perovskite Nanocrystals for Superior Optical Properties

Journal
Nano Letters, 19(4)

ISSN
1530-6984

Authors
Jurow, Matthew J
Morgenstern, Thomas
Eisler, Carissa
et al.

Publication Date
2019-04-10

DOI
10.1021/acs.nanolett.9b00122

Peer reviewed

NANO LETTERS

Letter

pubs.acs.org/NanoLett

Manipulating the Transition Dipole Moment of $CsPbBr_3$ Perovskite Nanocrystals for Superior Optical Properties

Matthew J. Jurow,[*,†,‡] Thomas Morgenstern,[§] Carissa Eisler,[∥] Jun Kang,[‡] Erika Penzo,[†] Mai Do,[†] Manuel Engelmayer,[§] Wojciech Osowiecki,[‡,∥] Yehonadav Bekenstein,[∥] Christopher Tassone,[⊥] Lin-Wang Wang,[‡] A. Paul Alivisatos,[‡,∥,#] Wolfgang Brütting,[*,§] and Yi Liu[*,†,‡]

[†]Molecular Foundry, Lawrence Berkeley National Laboratory, Berkeley, California 94720, United States

[‡]Materials Sciences Division, Lawrence Berkeley National Laboratory, Berkeley, California 94720, United States

[§]Institute of Physics, University of Augsburg, 86135 Augsburg, Germany

[∥]Department of Chemistry and Materials Science and Engineering, University of California, Berkeley, California 94720, United States

[⊥]SSRL Materials Science Division, SLAC National Accelerator Laboratory, 2575 Sand Hill Rd MS 69, Menlo Park, California 94025, United States

[#]Kavli Energy NanoScience Institute, Berkeley, California 94720, United States

Supporting Information

ABSTRACT: Colloidal cesium lead halide perovskite nanocrystals exhibit unique photophysical properties including high quantum yields, tunable emission colors, and narrow photoluminescence spectra that have marked them as promising light emitters for applications in diverse photonic devices. Randomly oriented transition dipole moments have limited the light outcoupling efficiency of all isotropic light sources, including perovskites. In this report we design and synthesize deep blue emitting, quantum confined, perovskite nanoplates and analyze their optical properties by combining angular emission measurements with back focal plane imaging and correlating the results with physical characterization. By reducing the dimensions of the nanocrystals and depositing them face down onto a substrate by spin coating, we orient the average transition dipole moment of films into the plane of the substrate and improve the emission properties for light emitting applications. We then exploit the sensitivity of the perovskite electronic transitions to the dielectric environment at the interface between the crystal and their surroundings to reduce the angle between the average transition dipole moment and the surface to only 14° and maximize potential light emission efficiency. This tunability of the electronic transition that governs light emission in perovskites is unique and, coupled with their excellent photophysical properties, introduces a valuable method to extend the efficiencies and applications of perovskite based photonic devices beyond those based on current materials.

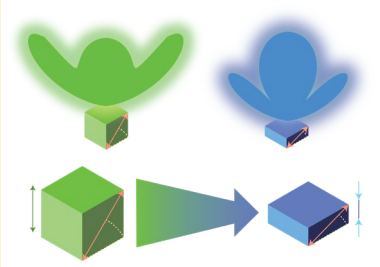

KEYWORDS: *2D materials, lead halide perovskite, LED, back focal plane imaging, transition dipole moment, anisotropic*

Cesium lead halide perovskite nanocrystals have demonstrated a suite of remarkable properties and show great promise as high-performance light emitters in applications including LEDs, general lighting, lasers, and displays.[1−9] Recent reports have provided synthetic pathways that allow for fine control of form factors, generating cubes, platelets, and wires spanning orders of magnitude in sizes, as well as control of emission colors by varying halide composition and particle dimensions above and below the Bohr exciton radius.[10−15]

Perovskite nanoparticles exhibit many unique and desirable photophysical properties generally attributed to their highly labile ligands, mobile halides, and band structure that imparts tolerance to surface defects, yielding particles with photoluminescent quantum yields (PLQY) above 90% without explicit shelling.[16−19] The absence of a shell of a wide band gap material preserves proximate physical access to electronic environment of the emissive material, making perovskite nanocrystals a unique platform to explore and tune the basic processes of light emission.

Even without any optimization of their emissive transition dipole moment, a vector that describes the polarization of an electronic transition between the emissive and ground state of a material, both hybrid organic and purely inorganic perovskites have demonstrated rapid progress as efficient light emitters in color tunable light emitting diodes (LEDs).[20−23] Electroluminescent perovskite-based LEDs have already achieved external quantum efficiencies (EQE) of 20.1%, trending rapidly toward values common in commercial displays.[24−29] Lead halide perovskites can emit light across the entire visible spectrum, including the blue region and do

Received: January 10, 2019
Revised: February 23, 2019
Published: March 8, 2019

DOI: 10.1021/acs.nanolett.9b00122
Nano Lett. XXXX, XXX, XXX−XXX

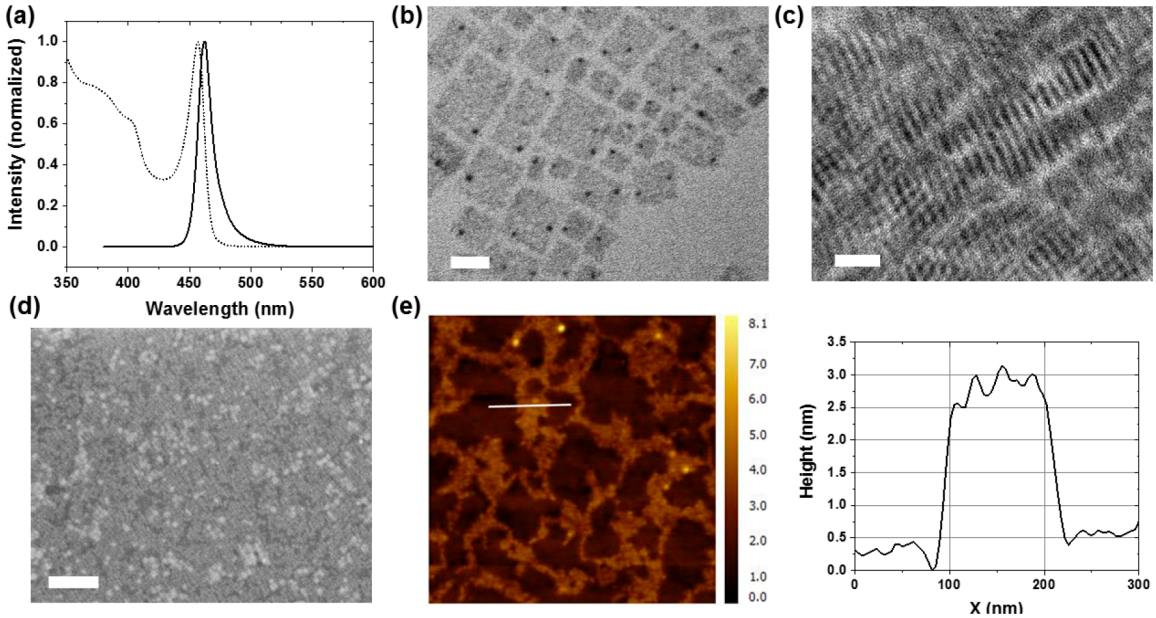

Figure 1. Characterization of nanoplate films. (a) Normalized photoluminescence (solid line) and absorbance (dashed line). Transmission electron microscopy (scale bar 20 nm) of films of nanoplates (b) face down and (c) on edge. (d) Scanning electron microscopy (scale bar 200 nm) and (e) atomic force microscopy of films of $CsPbBr_3$ nanoplates on silicon depicting face-down orientation of platelets on measured samples.

not rely on rare transition metals frequently featured in modern displays. Recent reports have also shown that perovskite nanoparticles owe their fast radiative decay and high brightness to their radiative lowest energy triplet state, the first ever observed in an inorganic semiconductor.[30] A bright triplet state offers a 4-fold potential EQE improvement in electroluminescent devices.

The introduction of oriented emitters has increased the EQE of modern OLEDs to almost 40%.[31−35] Anisotropic materials with oriented transition dipole moments will similarly be desirable to further improve the efficiency of quantum dot LEDs and present avenues to develop novel photonic devices.[36] Changing the interfaces between films of perovskite nanocubes has been shown to effect the average orientation of the transition dipoles.[18,23]

In the following report, we have synthesized colloidally stable, few layer thick, perovskite nanoplates and used them as blue light emitters with orientable transition dipole moments.[8,37−40] We employed both angular dependent photoluminescence and back focal plane imaging to unambiguously measure the orientation of the transition dipole moments in spin-cast films of perovskite nanoplates, finding excellent agreement between the techniques despite sampling at length scales that differ by orders of magnitude. By confining emissive excitons and orienting the nanoplates, we can significantly lower the angle of the average transition dipoles toward the plane of the substrate, thus greatly increasing the fraction of photons escaping the film. By then depositing a thin film of alumina on the exposed surface of the platelets we generate an additional electrostatic interaction that further directs the overall transition dipole moment to optimize the optical mode distribution of the emissive film. These results offer a valuable lever to tune the light emission properties of a bright and versatile nanocrystalline light emitter, as well as the tools required to understand the results.

Particle Synthesis and Characterization. $CsPbBr_3$ nanoplates were synthesized by the original published hot injection procedure,[8] which in turn is an adaptation of the original lead halide perovskite colloidal nanocrystal synthesis.[7] Briefly, cesium oleate was injected into a solution of lead oleate to yield approximately square monodisperse perovskite nanoplates (Figure 1).[8] Solutions of the resulting particles in toluene have a narrow photoluminescence peak at λ_{max} = 460 nm, a small Stokes shift with strong excitonic absorption peaks, and quantum yields generally above 70% (Figure 1a). The powder X-ray diffraction pattern of a drop cast film of the nanoplates matches well with the calculated spectrum from a bulk 3D perovskite crystal (Figure S1).[41] While some inner filter effects are expected, discrete emission maxima corresponding to isolated nanoplate thicknesses are occasionally observed because of the relative abundances of the species.[42] Purified nanoplates are approximately 15 nm on edge and 3 nm thick, composed of 4−5 monolayers or perovskite (Figure 1b,c,e).

Most lighting applications rely on solid films of materials. To create useful samples, films of nanoplates were then spin coated from colloidal suspensions in toluene, yielding tiled monolayers of nanoplates (Figure 1d). When spin-cast into films, small shifts in the photoluminescence peak are sometimes observed (Figure S7), and the quantum yield generally decreases by as much as 20% relative to the initial value. To quantify the degree of orientation of the perovskite nanocrystals, grazing incidence X-ray scattering measurements were performed (Figure 2). The sample exhibits strong texturing, with the (0*K*0) planes of the perovskite crystals preferentially oriented out of the substrate plane. The position of the Bragg spots agrees well with the calculated cubic perovskite geometry, and the (020), (121), (101), and (002) peaks are labeled (Figure S2).[8,41]

The nanoscale structure present within the thin film samples was probed using grazing incidence small angle scattering (GISAXS) (Figure 2a). Two features are present in the scattering pattern. The in-plane direction shows a characteristic Yoneda peak, while the out-of-plane direction exhibits a

DOI: 10.1021/acs.nanolett.9b00122
Nano Lett. XXXX, XXX, XXX−XXX

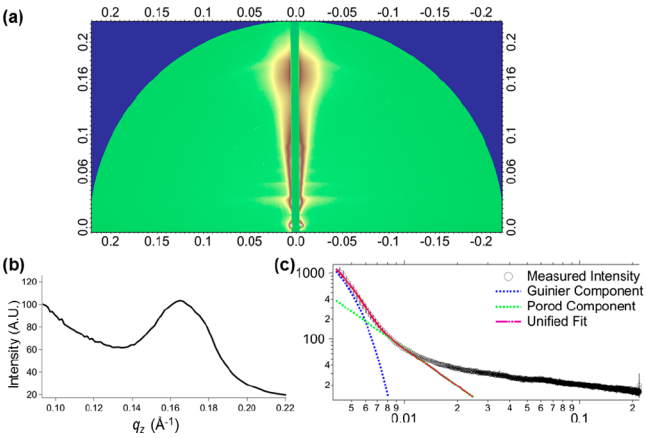

Figure 2. Grazing incidence small-angle X-ray scattering from films of perovskite nanoplates. (a) Grazing incidence small angle diffractogram. (b) Integration of the GISAXS pattern along q_z and (c) of the Yoneda peak are representative of a film of 3.8 nm nanoplates packed into ca. 150 nm tiled domains.

diffraction peak at finite q_z. Integration of the GISAXS pattern along the q_z direction (Figure 2b) clearly shows a broad diffraction peak centered at 1.65 nm^{-1}, corresponding to a correlation distance of 3.8 nm. We attribute this periodicity to the regions of the film that have overlapping multilayers of nanoplates. Integrating the Yoneda peak (Figure 2c), we observe an exponential decay that we fit with the unified fit approach.[43] Although we cannot clearly observe the Guinier plateau, we are able to achieve a reliable fit, which corresponds to a radius of gyration of 150 nm. We attribute this to the average domain size of continuous regions of the film. We do not observe diffraction, which would indicate long-range order of the nanocrystals in the plane of the film, and we believe that variations in plate size preclude long-range order, which would result in a Bragg peak.

Measuring the Orientation of Transition Dipole Moments. In materials that emit light by excitonic recombination, photons are emitted with a cosine angular distribution whose peak is oriented perpendicular to the transition dipole moment.[23] In an emissive material with a random distribution of transition dipole moments, the ensemble average over the measured area will exhibit equal components in (x, y, z) and photons are emitted isotropically. By reducing one dimension of a nanoparticle below the Bohr exciton radius to creating a 2D plate, we aim to restrict the transition dipole to the (x, y) plane. To orient emitted photons out of the plane of the substrate, we therefore need a layer of thin nanoplates lying face down on the substrate, achieved by spin coating from a colloidal suspension in toluene.[44]

To unambiguously quantify the orientation of the transition dipole moments we used an analysis of the angular dependence of the radiation pattern as well as back focal plane imaging, each coupled with the appropriate optical model.[18,45−48] We extract the alignment constant from the light emitted from the films of nanoplates using two different methods with different characteristics to avoid artifacts and unintended perturbations. By employing both of these methods together, we can study the orientation of emissive transitions on length scales ranging from millimeters to nanometers.

First, to quantify the orientation of emitted photons from continuous films of nanoplates, we mounted glass slides with the above-described submonolayer films of nanoplates onto a half-cylindrical prism, optically excited the film with an 18 mW 325 nm laser, and measured the intensity of emitted light at each angle around the periphery of the prism (Figure 3). This technique provides an ensemble measurement of the average transition dipoles of all emissive particles over the entire area excited (1 mm^2). To extract the anisotropy of the materials transition dipoles, the relationship of the emitted light intensity is simulated with a dipole radiation model in a 1D microcavity derived by Barnes et al.[45] This analysis provides the reported alignment constant ζ.[18] This parameter is bounded between 0 and 1 and quantifies the angular distribution of emitted power. An emissive film with perfectly horizontal transition dipole moments would produce a ζ value of 0, a film with all vertical transition dipoles would yield a ζ value of 1.

Critically, this factor is unique across materials with different refractive indices. The angle of the transition dipole moment with respect to the substrate can then be calculated from a given value of ζ and the refractive index of the emissive material according to eq 1.

$$\varphi = \operatorname{asin}\left(\sqrt{\frac{n^4\zeta}{1+\zeta(n^4-1)}}\right) \quad (1)$$

We approximate the refractive index of the material with a Bruggeman effective medium approach. The refractive indices of the emitting perovskite and the organic ligands are taken to be 2.3 and 1.45 respectively.[49−51] Averaging over the density of

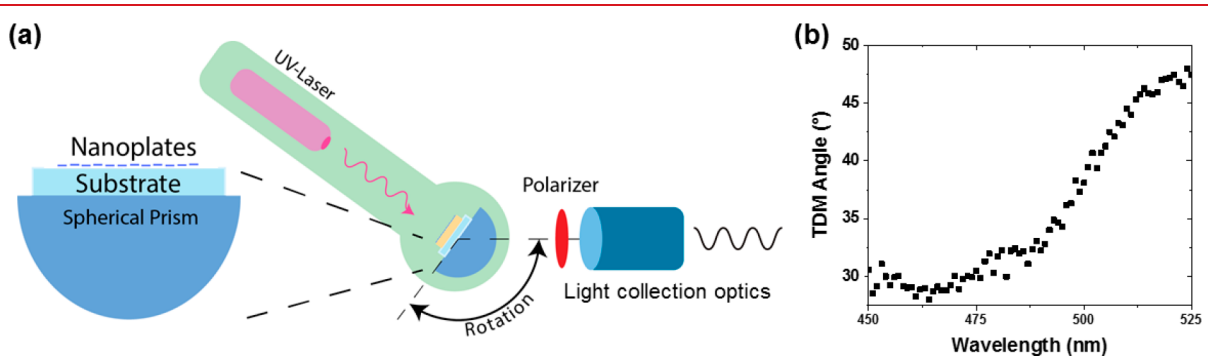

Figure 3. Measurement of angular dependent photoluminescence. (a) By mounting a film of perovskite nanoplates to a prism and analyzing the emitted light, we calculated the average orientation factor (ζ) of the material at each wavelength. (b) We found relatively horizontally oriented transition dipoles (refractive index 2.0) in films of quantum confined perovskite nanoplates that trend vertical as the emission approaches wavelengths associated with less confined particles during extended irradiation.

DOI: 10.1021/acs.nanolett.9b00122
Nano Lett. XXXX, XXX, XXX−XXX

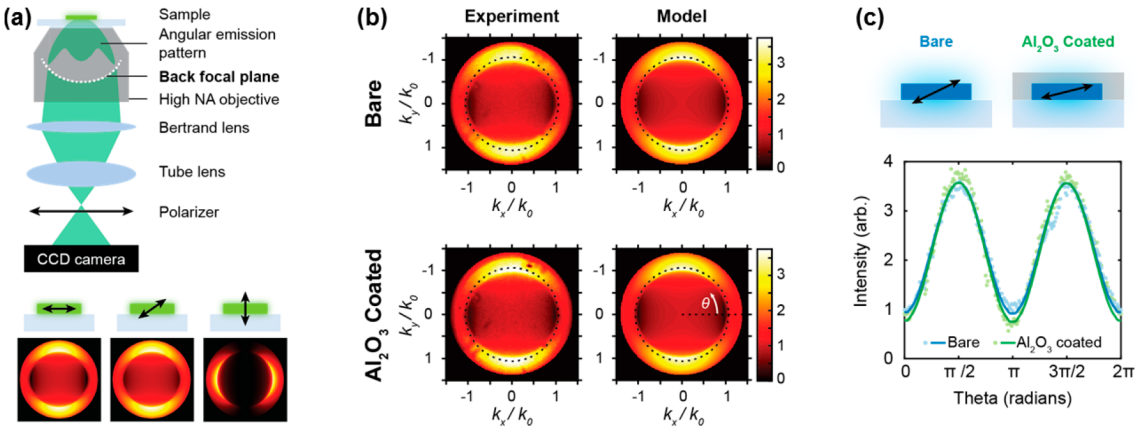

Figure 4. Oriented emission of bare and Al_2O_3 covered films of nanoplates analyzed with back focal plane imaging. (a) Schematic of the BFP measurement setup, including the Bertrand lens that changes the focus from the sample to the back focal plane, where the angular emission pattern of the sample is observed. Example of calculated BFP images for $\varphi = 0°$, isotropic, and 90° (below). (b) BFP images for bare (top) and Al_2O_3 coated (bottom) from the experiment and the model (center). The Al_2O_3 has a lower surface to transition dipole moment angle φ. (c) Intensity along the black dotted circles in the BFP images plotted along with calculated fits.

the close packed regions visible in electron microscopy (Figure 1, Supporting Information S5) we use an overall refractive index of 2.0 throughout this manuscript when assigning the dimensionless ζ term a physical meaning.

Surprisingly, the transition dipole moments of the perovskite nanoplates were not rigidly oriented in-plane as is observed for other 2D materials.[44] Light emitted at 460 nm from films of nanoplates yields a ζ value of 0.019. Equation 1 shows the relationship between the angle of the transition dipole moment with respect to the substrate (φ) and the alignment constant (ζ). Applying this equation yields an average angle of 29° between the surface and the transition dipole moment vector. For comparison, this value corresponds to a traditional (dependent on refractive index) orientation factor of Θ = 0.23 in the nomenclature commonly used for measuring OLEDs, nearly equivalent to those achieved for highly efficient acetyl acetonate containing iridium phosphors.[31,35]

Under the intense excitation employed in this measurement geometry, aggregates of nanoplates on the surface reconstruct, evidenced by broadening and red-shifting of the photoluminescence and the eventual growth of a new peak visible at 520 nm, the emission wavelength of the bulk material (see Supporting Information Figure S3).[7] When we extract the orientation factor of the transition dipole moments from these wavelengths, we observe an increase in the value of ζ. This increase arises because of the loss of confinement in the z direction as the nanoplates fuse (and thus thicken), eventually passing even the surface-transition dipole angle expected for isotropic light emitters (35.4°) and approaching values consistent with previous reports of the disproportionately vertical transition dipole moments observed in films of $CsPbBr_3$ perovskite nanocubes on surfaces.[18]

To then analyze light emission from a small targeted region of the surface and avoid sample degradation, we analyzed light emission from films of nanoplates using back focal plane imaging (BFP).[47,48] By employing a 405 nm diode laser focused down to a diffraction limited (200 nm) excitation spot, we measured light emitted from individual islands of packed particles. Results are shown in Figure 4. No plate fusion was observed during the measurement owing to the reduced power of the excitation source. By using a linear polarizer in front of the imaging pattern, we are able to fit the emission patterns to determine the dipole strengths, as in other work.[44] In this technique the back focal plane of a microscope objective is imaged, which shows the 2D projection of a sample's angular emission. This generates a circle where each point within the circle corresponds to a unique angle; the center of the circle represents normal emission (parallel to the optical axis) and the outer edge represents the maximum collection angle (here 77°, as determined by the numerical aperture). BFP has been used to determine the orientation of individual molecules and the average transition dipole moments observed in oriented films of anisotropic nanocrystals.[44,47]

The BFP image is a strong function of the overall angle of the average transition dipole moment, as shown by Figure 4. An angle of $\varphi = 0°$ has very pronounced minima, while a film of particles with purely vertical transitions ($\varphi = 90°$) shows very strong emission in this same location. In general, BFP images with lower, more pronounced minima are indicative of a lower transition dipole angle.

Analysis of back focal plane images from excited films of nanoplates resulted in a transition-dipole-moment-to-surface angle of 29 ± 1° (Figure 4c, blue line, normalized), in perfect agreement with the measurement obtained with our angular analysis. Fitting the full profile of the emission, rather than a linear cut, yields the small error bar on this measurement (see Supporting Information for details). These two techniques together allow us to understand the relationship of nanoscale organization, emission wavelength, and the orientation of the emissive transition on length scales spanning 3 orders of magnitude and show that by constricting the thickness of the nanocrystal we can successfully orient the transition dipole moment toward the plane of the substrate.

Controlling the Orientation of Transition Dipole Moments. An ideal light emitter with a perfectly two-dimensional transition dipole, i.e., lying flat on a substrate with a surface-transition angle of 0°, would yield a ζ value of 0. The nanoplates in our films are not perfectly quantum confined and are thus expected to deviate from ideal. Additionally, the interface of the exposed surface of the ionic nanoparticles and a higher work function oxide substrate creates an electrostatic charge that strongly enhances the z component of the transition dipole moment, responsible for the vertical average transition dipole observed in films of otherwise symmetric

DOI: 10.1021/acs.nanolett.9b00122
Nano Lett. XXXX, XXX, XXX−XXX

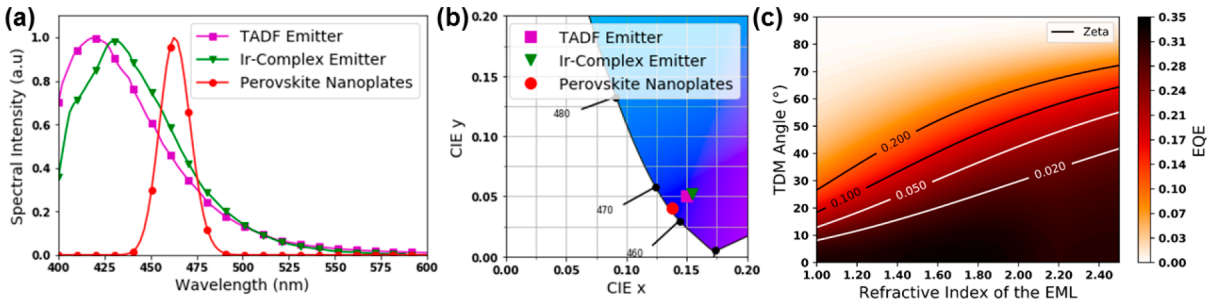

Figure 5. Perovskites as deep blue light emitters. The narrow emission band (a) of perovskite nanoplates produces deep blue CIE coordinates of (0.14, 0.04) (b). Particles are compared with contemporary organometallic and thermally activated delayed fluorescent blue emitters for context. (c) The high refractive index of the emissive material also increases the theoretical maximum EQE for perovskite-based light emitting diodes at a wider range of transition dipole angles.

nanocubes, and likely contributes to the larger transition-to-surface angle observed here relative to some semiconductor nanoplates.[18,44] We thus hypothesized that by introducing an additional surface/surface interaction on the top face of the emissive film, we should counterbalance the influence of the substrate, and further decrease the angle between the substrate and the transition dipole moment. Because of the uniquely accessible surface of the perovskite nanoparticle, we expected that the introduction of a material with a similar work function on the opposing face of the particle would create a comparable charge reconfiguration that would apply a field antiparallel to the distortion caused by the substrate. To create this system, we deposited a 3 nm layer of alumina using a plasma deposition process onto the top of the emissive layer. This process has been detailed elsewhere and has been shown to improve the long-term stability of films of perovskite nanoparticles.[52]

After the deposition of the Al_2O_3 layer, the fitted average transition dipole to surface angle decreases by more than 50% to only 14 ± 4° (Figure 4, green line, normalized). An LED made from this system has a potential maximum efficiency of 31.7%. For comparison, an isotropic emitter in the same stack would yield a maximum potential EQE of only 25.8%. For clarity, we plotted the intensity as a function of θ along the dotted black circle. The Al_2O_3 coated samples have a lower intensity than the bare samples at 0, π, and 2π, showing that the transition dipole angles to the surface are reduced. We then fit the entire BFP image to determine the ratio of in- and out-of-plane dipoles, and therefore the average transition dipole moment. The fitted models show good agreement to the experimental BFP images.

The experimental confirmation of the tunability of the average transition dipole moment in films of bright perovskite nanoparticles presents a fascinating pathway toward efficient photonic devices. The agreement of the two distinct optical measurements is encouraging. Finally, the demonstrated ability to improve the optical mode distribution is unique to perovskites and will motivate further exploration of perovskite based photonic devices.

Impact on Light Sources. Limiting the physical size of the nanocrystal below the Bohr exciton radius, even in only one dimension, effectively confines the exciton and induces a ca. 55 nm hypsochromic shift relative to larger $CsPbBr_3$ nanocrystals.[7] Critically, this deep blue emission is achieved without employing anion substitution that decreases the stability and quantum yield of an already fragile material. By creating quantum confined particles, light emitted from films of nanoplates is thus within the display blue range, featuring CIE coordinates (0.14, 0.04) (Figure 5b). The remarkably low CIE y is due to the narrow emission peak, an advantage of perovskite light emitters relative to state of the art light emitters including recently reported Ir complexes[53] or TADF emitters[54] (Figure 5a).[55] Despite substantial challenges, access to deep blue emission provides motivation to continue the device engineering and injection/interface material development required to create stable electroluminescent perovskite devices.

To better assess the potential value of perovskite nanoplates as light sources, we performed optical simulations using a classical dipole model with a matrix transfer formalism as described in earlier publications (see Supporting Information).[45,56,57] The emissive transition is modeled as a classical dipole trapped within a one-dimensional microcavity between the substrate and vacuum. If applied to a full device stack, this technique allows for the evaluation of the different emission channels within the light emitting device.

The outcoupling efficiency of a microcavity, such as a light emitting device, is determined by several key factors including the angle of the emissive TDM with respect to the surface, the refractive indices of the materials involved, and the film thicknesses. Each layer thicknesses of the modeled stack layout (see Supporting Information for details of model device architecture) was optimized to maximize the outcoupling efficiency by suppressing destructive interference inside the system. Afterward, the optimized layout was calculated for variations of both the refractive index of the emissive film as well as the angle of the emissive transition dipole moment, yielding a two-dimensional map of device efficiencies as shown in Figure 5c. Decreasing the angle of the emissive transition dipole consequently leads to more efficient outcoupling, as expected. However, an increase of the refractive index further enhances the amount of light leaving the system. This counterintuitive behavior can be understood via the loss channels to wave guided modes and surface plasmon polaritons shown in Figure S4. Although the contribution to wave guided modes is increased by the refractive index, the loss is compensated for by a decrease in the surface plasmon polaritons. The combined effect of both transition dipole moment and refractive index can be quantified by the alignment constant ζ, yielding the maximum possible device efficiency for a given emissive system. The remarkably low ζ value of 0.02 allows perovskite nanoplates to outperform many common organic emissive systems. It is important to note that

DOI: 10.1021/acs.nanolett.9b00122
Nano Lett. XXXX, XXX, XXX−XXX

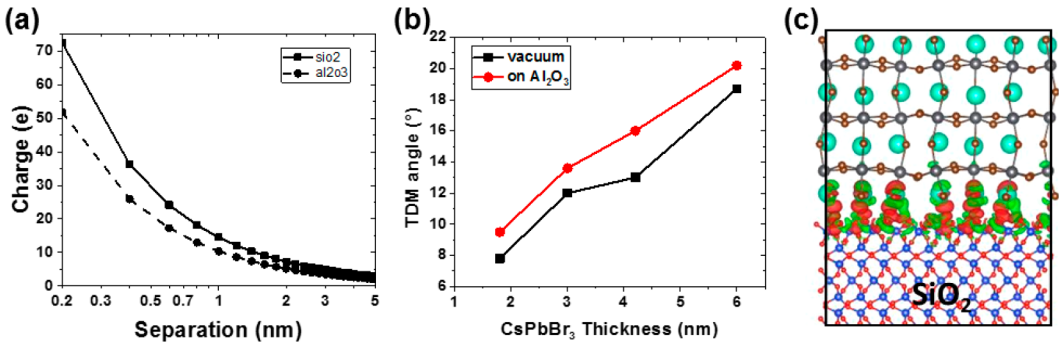

Figure 6. Modeling the perovskite−substrate interface. (a) Plot of the relationship between the particle/substrate separation and the resulting electrostatic surface charge. (b) DFT trends of the transition dipole moment to surface angle φ as a function of plate thickness both in a vacuum and in contact with an oxide surface. As a nanoplate becomes thicker the z component of the transition dipole moment is strengthened and the angle between the transition and the substrate (φ) increases. (c) Depiction of the resulting charge recombination region at the nanoparticle/substrate interface.

this effect depends on the thickness of the nanoplates and can be lost in device geometries with thicker emissive layers.

Theoretical Modeling. To approximate the magnitude of the surface charge between the nanoplate and the substrate, we modeled the system as two semiconductors in contact, assuming work functions: SiO_2 (5 eV), Al_2O_3 (4.7 eV), and $CsPbBr_3$ (3.95 eV).[58] The charge created by bringing a perovskite surface into contact with a substrate is then given by eq 2 where the charge per unit area (Q/S) is the permittivity of free space (ε_0) divided by the distance between the surfaces multiplied by the difference between the work functions of the materials. The results of this calculation are plotted in Figure 6 and are somewhat intuitive, showing a strong surface charge when the particles are in close contact with the silica (or alumina) that rapidly diminishes as the separation increases, suggesting that less labile or thicker ligand shelling may reduce the sensitivity of the particles transition dipole moments to their surroundings. The corresponding field strength at this interface rapidly exceeds thousands of V/μm and should easily manipulate the distribution of the transition dipole moment.

$$\frac{Q}{S} = \frac{\varepsilon_r}{d}\Phi_{a-b} \tag{2}$$

Beyond the quantification of the electrostatics, to calculate the probable orientation of the transition dipole moment we modeled the nanoplates as infinite $CsPbBr_3$ slabs with Cs-terminated (100) surfaces. The transition dipole along the α direction is calculated by $p_\alpha = |\varphi_{CBM}|i\nabla_\alpha|\varphi_{VBM}|^2$, where $\alpha = x, y, z$. The polarization angle φ is defined as $\varphi = \mathrm{atan}[p_z/(p_x + p_y)]$. The details of the DFT calculation are given in the Supporting Information. For a freestanding 4.2 nm thick nanoplate, φ is calculated to be 13°. When the same quantity is calculated for a nanoplate in close contact with a silica substrate, φ increased to 16° due to the charge redistribution caused by the electric field gradient. We calculated the φ thickness dependence for nanoplates both in a vacuum and on surfaces (Figure 6). As the thickness of the plate increases, thus weakening the confinement of the exciton, φ also increases. This result is intuitive at the limits; when the thickness trends to infinity, the transition dipole moment angles trend toward the value observed in nanocubes. Despite the trend, the calculated values differ from reality because the modeled plate must have a periodic boundary condition along the x and y directions, where the real plate has a finite length along x and y. This increases the calculated angle for the isolated plate and will motivate development of a more precise model in the future in which we hope to better represent the critical local dielectric environment.

Assuming a constant separation distance of 5 Å, the calculated electrostatic reorganization created at a perovskite/silicon dioxide interface is 0.012 e/Å^2, while the same interface with a lower work function alumina coating creates differential of 0.008 e/Å^2. Thus, we can understand the observed reduction in the average transition dipole moment angle of the film as the result of the introduction of an antiparallel charge redistribution that moves the system closer to the ideal. This result also suggests that introduction of a very high work function coating could further manipulate the transition dipoles to yield still better films, and we are continuing to develop the ALD processes to deposit more diverse coatings.

Conclusions. We synthesized $CsPbBr_3$ perovskite nanoplates with confined excitons to create efficient deep blue emission. The narrow emission line results in CIE coordinates of (0.14, 0.04). By then orienting films of these high aspect ratio quasi 2D particles, we can orient their average transition dipole moments into the plane of the substrate and improve the optical mode distribution of the emitted light. In perovskite nanostructures, the transition dipole moment is impacted by the interaction between the particle and the substrate because of the proximal access to the electronic environment of the emitter, providing a unique lever to tune the orientation of the transition and thus the characteristics of emitted light. We take advantage of this accessibility by overcoating the emissive particles with a thin transparent layer of alumina and further reducing the angle between the transition dipoles and the substrate by more than 50% to only 14°. The resulting films have potential device efficiencies well beyond the limits of isotropic light sources. This type of in situ control of an emissive transition dipole moment in a color tunable material is unique to perovskites, demonstrates great promise for future applications in displays and photonic devices and will motivate future work on other interfacial techniques to improve perovskite light sources.

DOI: 10.1021/acs.nanolett.9b00122
Nano Lett. XXXX, XXX, XXX−XXX

■ ASSOCIATED CONTENT

Supporting Information

The Supporting Information is available free of charge on the ACS Publications website at DOI: 10.1021/acs.nanolett.9b00122.

Material characterization, materials used, synthetic and deposition procedures, X-ray scattering spectra, angle dependent emission measurements, optical modeling, back focal plane imaging, and error analysis (PDF)

■ AUTHOR INFORMATION

Corresponding Authors

*Matthew Jurow. E-mail: mjurow@lbl.gov. Telephone: 510-486-7728. Fax: 510-486-7413.

*Wolfgang Brütting. E-mail: Wolfgang.bruetting@physik.uni-augsburg.de. Telephone: ++49 (0)821-598-3403. Fax: ++49 (0)821-598-3425.

*Yi Liu. E-mail: yliu@lbl.gov. Telephone: 510-486-6287. Fax: 510-486-7413.

ORCID

Matthew J. Jurow: 0000-0003-3943-4765

Wojciech Osowiecki: 0000-0002-7051-1768

A. Paul Alivisatos: 0000-0001-6895-9048

Wolfgang Brütting: 0000-0001-9895-8281

Yi Liu: 0000-0002-3954-6102

Author Contributions

The manuscript was written through contributions of all authors. All authors have given approval to the final version of the manuscript.

Notes

The authors declare no competing financial interest.

■ ACKNOWLEDGMENTS

The authors thank Matthew Kolaczkowski for his generous assistance with atomic force microscopy. This work was supported by the U.S. Department of Energy, Office of Science, Office of Basic Energy Sciences, Materials Sciences and Engineering Division, under Contract No. DE-AC02-05-CH11231 within the Inorganic/Organic Nanocomposites Program (KC3104) (materials synthesis, sample preparation, and analysis). Work at the Molecular Foundry was supported by the Office of Science, Office of Basic Energy Sciences, of the U.S. Department of Energy under Contract No. DE-AC02-05CH11231. Use of the Stanford Synchrotron Radiation Light Source, SLAC National Accelerator Laboratory, is supported by the U.S. Department of Energy, Office of Science, Office of Basic Energy Sciences under Contract No. DE-AC02-76SF00515. T.M., M.E., and W.B. acknowledge financial support by Bavaria California Technology Center (BaCaTeC), by the German Ministry for Education and Research (BMBF, Project no. 13N14422), and by Deutsche Forschungsgemeinschaft (DFG, Project nos. Br 1728/18&20).

■ REFERENCES

(1) Colella, S.; Mazzeo, M.; Rizzo, A.; Gigli, G.; Listorti, A. *J. Phys. Chem. Lett.* **2016**, *7* (21), 4322−4334.

(2) Sutherland, B. R.; Sargent, E. H. *Nat. Photonics* **2016**, *10* (5), 295−302.

(3) Swarnkar, A.; Chulliyil, R.; Ravi, V. K.; Irfanullah, M.; Chowdhury, A.; Nag, A. *Angew. Chem., Int. Ed.* **2015**, *54* (51), 15424−15428.

(4) Yoon, H. C.; Kang, H.; Lee, S.; Oh, J. H.; Yang, H.; Do, Y. R. *ACS Appl. Mater. Interfaces* **2016**, *8* (28), 18189−18200.

(5) Pan, A.; Wang, J.; Jurow, M. J.; Jia, M.; Liu, Y.; Wu, Y.; Zhang, Y.; He, L.; Liu, Y. *Chem. Mater.* **2018**, *30* (8), 2771−2780.

(6) Nurmikko, A. *Nat. Nanotechnol.* **2015**, *10* (12), 1001−1004.

(7) Protesescu, L.; Yakunin, S.; Bodnarchuk, M. I.; Krieg, F.; Caputo, R.; Hendon, C. H.; Yang, R. X.; Walsh, A.; Kovalenko, M. V. *Nano Lett.* **2015**, *15* (6), 3692−3696.

(8) Bekenstein, Y.; Koscher, B. A.; Eaton, S. W.; Yang, P.; Alivisatos, A. P. *J. Am. Chem. Soc.* **2015**, *137* (51), 16008−16011.

(9) Akkerman, Q. A.; Rainò, G.; Kovalenko, M. V.; Manna, L. *Nat. Mater.* **2018**, *17* (5), 394−405.

(10) Pan, A.; He, B.; Fan, X.; Liu, Z.; Urban, J. J.; Alivisatos, A. P.; He, L.; Liu, Y. *ACS Nano* **2016**, *10* (8), 7943−7954.

(11) Imran, M.; Caligiuri, V.; Wang, M.; Goldoni, L.; Prato, M.; Krahne, R.; De Trizio, L.; Manna, L. *J. Am. Chem. Soc.* **2018**, *140* (7), 2656−2664.

(12) Shamsi, J.; Dang, Z.; Bianchini, P.; Canale, C.; Stasio, F. D.; Brescia, R.; Prato, M.; Manna, L. *J. Am. Chem. Soc.* **2016**, *138*, 7240.

(13) Zhang, D.; Eaton, S. W.; Yu, Y.; Dou, L.; Yang, P. *J. Am. Chem. Soc.* **2015**, *137* (29), 9230−9233.

(14) Yang, Y.; Gao, F.; Gao, S.; Wei, S.-H. *J. Mater. Chem. A* **2018**, *6*, 14949.

(15) Bohn, B. J.; Tong, Y.; Gramlich, M.; Lai, M. L.; Döblinger, M.; Wang, K.; Hoye, R. L. Z.; Müller-Buschbaum, P.; Stranks, S. D.; Urban, A. S.; Polavarapu, L.; Feldmann, J. *Nano Lett.* **2018**, *18*, 5231.

(16) Kang, J.; Wang, L.-W. *J. Phys. Chem. Lett.* **2017**, *8*, 489−493.

(17) De Roo, J.; Ibáñez, M.; Geiregat, P.; Nedelcu, G.; Walravens, W.; Maes, J.; Martins, J. C.; Van Driessche, I.; Kovalenko, M. V.; Hens, Z. *ACS Nano* **2016**, *10* (2), 2071−2081.

(18) Jurow, M. J.; Lampe, T.; Penzo, E.; Kang, J.; Koc, M. A.; Zechel, T.; Nett, Z.; Brady, M.; Wang, L.-W.; Alivisatos, A. P.; Cabrini, S.; Brütting, W.; Liu, Y. *Nano Lett.* **2017**, *17* (7), 4534−4540.

(19) Goesten, M. G.; Hoffmann, R. *J. Am. Chem. Soc.* **2018**, *140*, 12996.

(20) Kumawat, N. K.; Dey, A.; Kumar, A.; Gopinathan, S. P.; Narasimhan, K. L.; Kabra, D. *ACS Appl. Mater. Interfaces* **2015**, *7* (24), 13119−13124.

(21) Gong, X.; Voznyy, O.; Jain, A.; Liu, W.; Sabatini, R.; Piontkowski, Z.; Walters, G.; Bappi, G.; Nokhrin, S.; Bushuyev, O.; Yuan, M.; Comin, R.; McCamant, D.; Kelley, S. O.; Sargent, E. H. *Nat. Mater.* **2018**, *17* (6), 550−556.

(22) Li, J.; Shan, X.; Bade, S. G. R.; Geske, T.; Jiang, Q.; Yang, X.; Yu, Z. *J. Phys. Chem. Lett.* **2016**, *7* (20), 4059−4066.

(23) Turro, N. J. *Modern molecular photochemistry of organic molecules*; University Science Books: Sausalito, CA, 2010.

(24) Li, J.; Xu, L.; Wang, T.; Song, J.; Chen, J.; Xue, J.; Dong, Y.; Cai, B.; Shan, Q.; Han, B.; Zeng, H. *Adv. Mater.* **2017**, *29*, 1603885.

(25) Song, J.; Li, J.; Li, X.; Xu, L.; Dong, Y.; Zeng, H. *Adv. Mater.* **2015**, *27* (44), 7162−7167.

(26) Kim, Y.-H.; Wolf, C.; Kim, Y.-T.; Cho, H.; Kwon, W.; Do, S.; Sadhanala, A.; Park, C. G.; Rhee, S.-W.; Im, S. H.; Friend, R. H.; Lee, T.-W. *ACS Nano* **2017**, *11* (7), 6586−6593.

(27) Kumawat, N. K.; Swarnkar, A.; Nag, A.; Kabra, D. *J. Phys. Chem. C* **2018**, *122*, 13767.

(28) Lee, S.; Koo, H.; Kwon, O.; Jae Park, Y.; Choi, H.; Lee, K.; Ahn, B.; Min Park, Y. *Sci. Rep.* **2017**, *7* (1), 11995.

(29) Zhao, B.; Bai, S.; Kim, V.; Lamboll, R.; Shivanna, R.; Auras, F.; Richter, J. M.; Yang, L.; Dai, L.; Alsari, M.; She, X.-J.; Liang, L.; Zhang, J.; Lilliu, S.; Gao, P.; Snaith, H. J.; Wang, J.; Greenham, N. C.; Friend, R. H.; Di, D. *Nat. Photonics* **2018**, *12* (12), 783−789.

(30) Becker, M. A.; Vaxenburg, R.; Nedelcu, G.; Sercel, P. C.; Shabaev, A.; Mehl, M. J.; Michopoulos, J. G.; Lambrakos, S. G.; Bernstein, N.; Lyons, J. L.; Stöferle, T.; Mahrt, R. F.; Kovalenko, M. V.; Norris, D. J.; Rainò, G.; Efros, A. L. *Nature* **2018**, *553*, 189.

(31) Schmidt, T. D.; Lampe, T.; Sylvinson, M.; R, D.; Djurovich, P. I.; Thompson, M. E.; Brütting, W. *Phys. Rev. Appl.* **2017**, *8* (3), 037001.

DOI: 10.1021/acs.nanolett.9b00122
Nano Lett. XXXX, XXX, XXX−XXX

(32) Kim, S.-Y.; Jeong, W.-I.; Mayr, C.; Park, Y.-S.; Kim, K.-H.; Lee, J.-H.; Moon, C.-K.; Brütting, W.; Kim, J.-J. *Adv. Funct. Mater.* **2013**, *23* (31), 3896−3900.
(33) Kim, K.-H.; Moon, C.-K.; Lee, J.-H.; Kim, S.-Y.; Kim, J.-J. *Adv. Mater.* **2014**, *26* (23), 3844−3847.
(34) Kim, K.-H.; Liao, J.-L.; Lee, S. W.; Sim, B.; Moon, C.-K.; Lee, G.-H.; Kim, H. J.; Chi, Y.; Kim, J.-J. *Adv. Mater.* **2016**, *28* (13), 2526−2532.
(35) Jurow, M. J.; Mayr, C.; Schmidt, T. D.; Lampe, T.; Djurovich, P. I.; Brutting, W.; Thompson, M. E. *Nat. Mater.* **2016**, *15* (1), 85−91.
(36) Dai, X.; Zhang, Z.; Jin, Y.; Niu, Y.; Cao, H.; Liang, X.; Chen, L.; Wang, J.; Peng, X. *Nature* **2014**, *515*, 96.
(37) Butkus, J.; Vashishtha, P.; Chen, K.; Gallaher, J. K.; Prasad, S. K. K.; Metin, D. Z.; Laufersky, G.; Gaston, N.; Halpert, J. E.; Hodgkiss, J. M. *Chem. Mater.* **2017**, *29* (8), 3644−3652.
(38) Weidman, M. C.; Goodman, A. J.; Tisdale, W. A. *Chem. Mater.* **2017**, *29* (12), 5019−5030.
(39) Liang, D.; Peng, Y.; Fu, Y.; Shearer, M. J.; Zhang, J.; Zhai, J.; Zhang, Y.; Hamers, R. J.; Andrew, T. L.; Jin, S. *ACS Nano* **2016**, *10* (7), 6897−6904.
(40) Yang, D.; Zou, Y.; Li, P.; Liu, Q.; Wu, L.; Hu, H.; Xu, Y.; Sun, B.; Zhang, Q.; Lee, S.-T. *Nano Energy* **2018**, *47*, 235−242.
(41) Cottingham, P.; Brutchey, R. L. *Chem. Commun. (Cambridge, U. K.)* **2016**, *52* (30), 5246−5249.
(42) Koc, M. A.; Raja, S. N.; Hanson, L. A.; Nguyen, S. C.; Borys, N. J.; Powers, A. S.; Wu, S.; Takano, K.; Swabeck, J. K.; Olshansky, J. H.; Lin, L.; Ritchie, R. O.; Alivisatos, A. P. *ACS Nano* **2017**, *11* (2), 2075−2084.
(43) Beaucage, G. J. *J. Appl. Crystallogr.* **1996**, *29* (2), 134−146.
(44) Gao, Y.; Weidman, M. C.; Tisdale, W. A. *Nano Lett.* **2017**, *17* (6), 3837−3843.
(45) Barnes, W. L. *J. Mod. Opt.* **1998**, *45* (4), 661−699.
(46) Frischeisen, J.; Yokoyama, D.; Endo, A.; Adachi, C.; Brütting, W. *Org. Electron.* **2011**, *12* (5), 809−817.
(47) Lieb, M. A.; Zavislan, J. M.; Novotny, L. *J. Opt. Soc. Am. B* **2004**, *21* (6), 1210−1215.
(48) Schuller, J. A.; Karaveli, S.; Schiros, T.; He, K.; Yang, S.; Kymissis, I.; Shan, J.; Zia, R. *Nat. Nanotechnol.* **2013**, *8*, 271.
(49) Yakunin, S.; Protesescu, L.; Krieg, F.; Bodnarchuk, M. I.; Nedelcu, G.; Humer, M.; De Luca, G.; Fiebig, M.; Heiss, W.; Kovalenko, M. V. *Nat. Commun.* **2015**, *6*, 8056.
(50) Park, K.; Lee, J. W.; Kim, J. D.; Han, N. S.; Jang, D. M.; Jeong, S.; Park, J.; Song, J. K. *J. Phys. Chem. Lett.* **2016**, *7* (18), 3703−3710.
(51) Bernardo-Gil, G.; Esquivel, M.; Ribeiro, A. *J. Chem. Eng. Data* **1990**, *35* (2), 202−204.
(52) Loiudice, A.; Saris, S.; Oveisi, E.; Alexander, D. T. L.; Buonsanti, R. *Angew. Chem., Int. Ed.* **2017**, *56*, 10696.
(53) Pal, A. K.; Krotkus, S.; Fontani, M.; Mackenzie, C. F. R.; Cordes, D. B.; Slawin, A. M. Z.; Samuel, I. D. W.; Zysman-Colman, E. *Adv. Mater.* **2018**, *30*, 1804231.
(54) Chan, C.-Y.; Cui, L.-S.; Kim, J. U.; Nakanotani, H.; Adachi, C. *Adv. Funct. Mater.* **2018**, *28* (11), 1706023.
(55) Ithurria, S.; Tessier, M. D.; Mahler, B.; Lobo, R. P. S. M.; Dubertret, B.; Efros, A. L. *Nat. Mater.* **2011**, *10*, 936.
(56) Brütting, W.; Frischeisen, J.; Schmidt, T. D.; Scholz, B. J.; Mayr, C. *Phys. Status Solidi A* **2013**, *210* (1), 44−65.
(57) Penninck, L.; De Visschere, P.; Beeckman, J.; Neyts, K. *Opt. Express* **2011**, *19* (19), 18558−18576.
(58) Kulbak, M.; Gupta, S.; Kedem, N.; Levine, I.; Bendikov, T.; Hodes, G.; Cahen, D. *J. Phys. Chem. Lett.* **2016**, *7* (1), 167−172.

DOI: 10.1021/acs.nanolett.9b00122
Nano Lett. XXXX, XXX, XXX−XXX